

**NASA CONTRACTOR  
REPORT**



**NASA CR-10**

*2.1*

0060417



**NASA CR-1052**

**LOAN COPY: RETURN TO  
AFWL (WLIL-2)  
KIRTLAND AFB, N MEX**

**THE TEM RADIATION PATTERN OF  
A THIN-WALLED PARALLEL-PLATE  
WAVEGUIDE ANALYZED BY A  
SURFACE INTEGRATION TECHNIQUE**

*by D. C. F. Wu*

*Prepared by*  
**THE OHIO STATE UNIVERSITY**  
Columbus, Ohio

*for*

**NATIONAL AERONAUTICS AND SPACE ADMINISTRATION • WASHINGTON, D. C. • MAY 1968**

NASA CR-1052  
TECH LIBRARY KAFB, NM



0060417

THE TEM RADIATION PATTERN OF A THIN-WALLED  
PARALLEL-PLATE WAVEGUIDE ANALYZED BY  
A SURFACE INTEGRATION TECHNIQUE

By D. C. F. Wu

Distribution of this report is provided in the interest of information exchange. Responsibility for the contents resides in the author or organization that prepared it.

Issued by Originator as Technical Report No. 1691-23

Prepared under Grant No. NsG-448 by  
THE OHIO STATE UNIVERSITY  
Columbus, Ohio

for

NATIONAL AERONAUTICS AND SPACE ADMINISTRATION

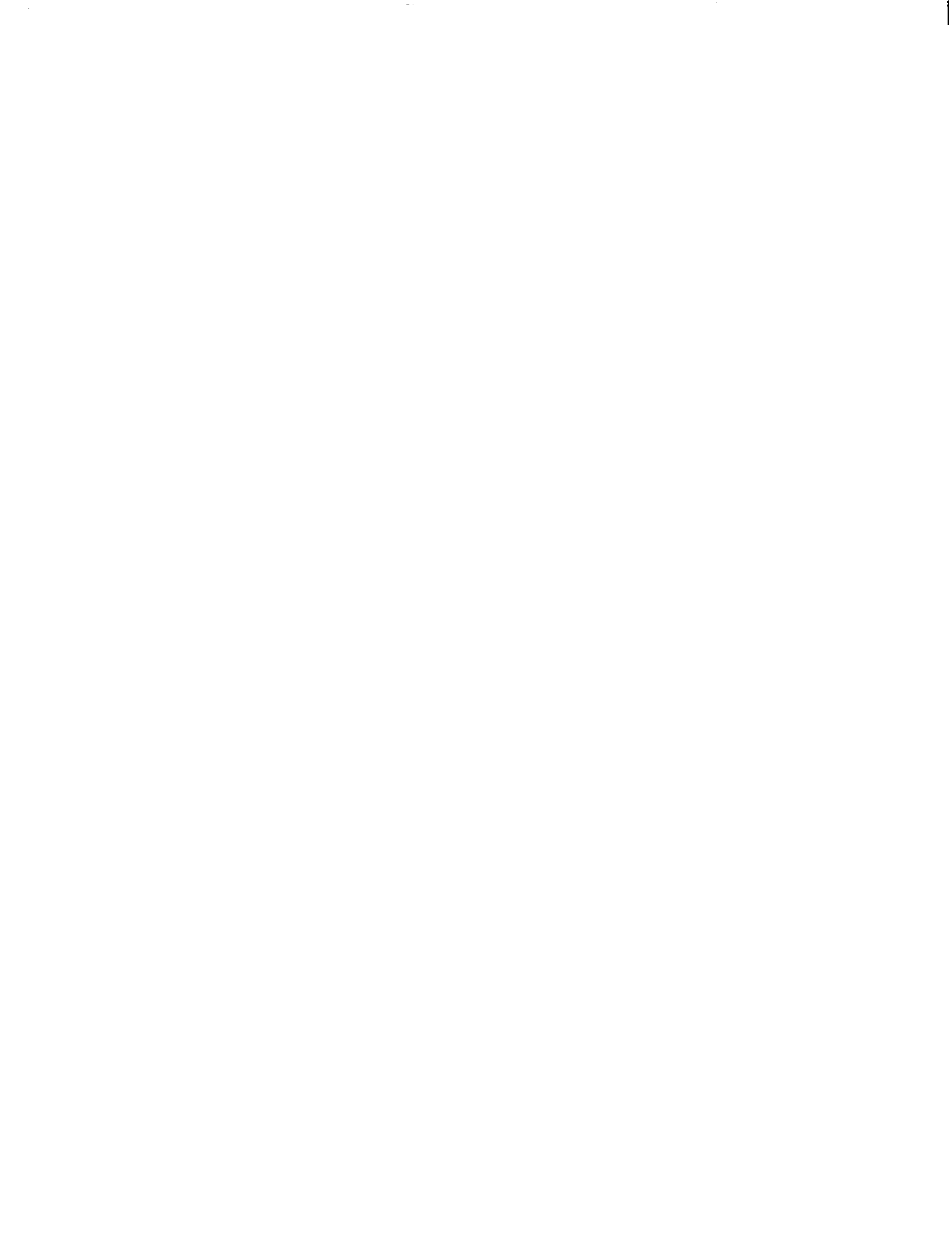
---

For sale by the Clearinghouse for Federal Scientific and Technical Information  
Springfield, Virginia 22151 - CFSTI price \$3.00



## ACKNOWLEDGMENTS

The author wishes to express his sincere gratitude to all those persons who provided assistance in bringing this thesis to its present state. Special thanks is extended to my advisor, Professor Roger C. Rudduck whose guidance and encouragement were invaluable. Particular thanks are given to Professors Carlton H. Walter and Robert G. Kouyoumjian for their advice and suggestions; Mr. Leonard L. Tsai and Mr. Walter D. Burnside for reviewing the manuscript.



## ABSTRACT

The radiation pattern of a TEM mode thin-walled parallel-plate waveguide is analyzed by a surface integration technique in conjunction with wedge diffraction theory. The surface integral is obtained by the Green's second identity. The fields on the surface are calculated by plane wave diffraction and first order interactions between two edges of the guide (which were employed in a previous pattern analysis by the wedge diffraction method). The surface integration technique provides an improvement in the accuracy of the pattern as compared to the wedge diffraction method.



## CONTENTS

Chapter		Page
I	INTRODUCTION	1
II	FORMULATION OF HALF-SPACE RADIATION IN TERMS OF SURFACE INTEGRAL	5
III	PLANE WAVE DIFFRACTION BY A HALF PLANE	9
	A. <u>Half-Plane Diffraction Formulation</u>	9
	B. <u>Surface Integral Representation</u>	11
IV	THE RADIATION PATTERN OF A TEM MODE PARALLEL-PLATE WAVEGUIDE	17
V	CONCLUSIONS	38
	APPENDIX A	39
	APPENDIX B	44
	REFERENCES	46

## CHAPTER I INTRODUCTION

Radiation pattern analysis is a primary tool in the design of antennas. Consequently, the development and improvement of methods of analysis are of particular interest to the antenna designer. Small aperture antennas such as open-ended waveguides and slot antennas are of particular interest in applications for missiles, space crafts, and airborne and reentry vehicles. The idealized two-dimensional parallel-plate waveguide which is treated below provides insight into the diffraction behavior of practical three-dimensional antennas. The research reported here provides an improvement in the accuracy of the parallel-plate guide pattern as compared to the wedge diffraction method.

Wedge diffraction theory has been previously applied to analyze the electromagnetic characteristics of waveguides and horn antennas.<sup>1, 2, 3</sup> Although the wedge diffraction method generally gives accurate results, limitations on accuracy occur under certain conditions. Specifically, in the wedge diffraction analysis of the radiation pattern of the TEM parallel-plate waveguide, as shown in Fig. 1, the result is not accurate in the region near the plane of the aperture especially for guide widths on the order of  $\lambda/2$  or less.

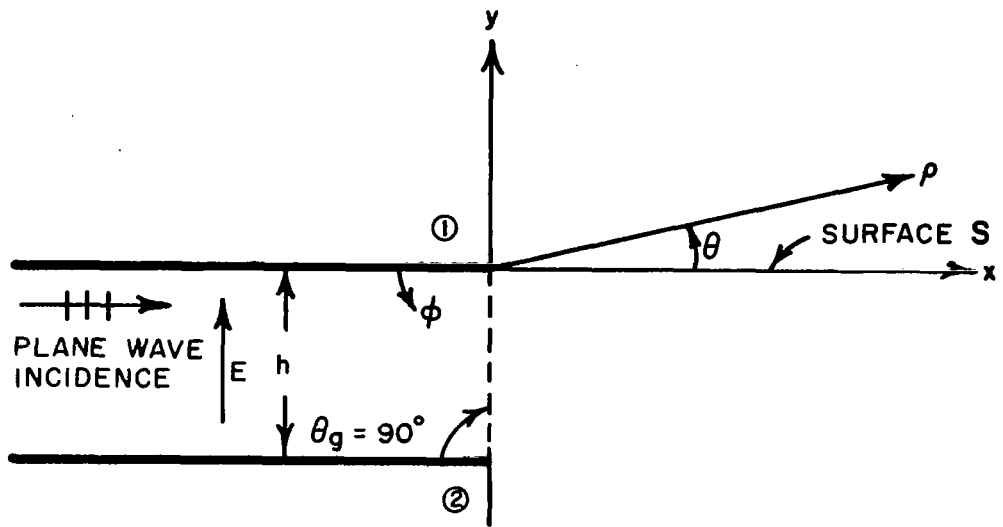


Fig. 1. Geometry of parallel-plate waveguide.

The purpose of the development in this publication is to establish a method of antenna analysis which overcomes the limitations of previous applications of wedge diffraction theory. The technique used in the research reported here employs an integration involving the fields over the surface represented by the x-axis in Fig. 1. The same basic approach has been used by Mikuteit<sup>4</sup> in the analysis of coupling in a three-guide array.

The validity of this technique is demonstrated by the improved accuracy of the radiation pattern analysis for this problem as compared with the wedge diffraction analysis. The basis for the comparison is the known exact solution.

It is believed that this method provides a means for similar improvement of the accuracy of the radiation pattern analysis for a waveguide mounted in an infinite ground plane. There is no exact solution known for this case. The radiation pattern for the waveguide in an infinite ground plane is now being analyzed and will be presented in a later publication.

In the wedge diffraction method, the incident plane wave causes singly diffracted waves to emanate from edges (1) and (2) as shown in Fig. 1. Doubly diffracted waves are produced by the incidence of the singly diffracted waves on the opposite edges. The doubly diffracted wave is approximated as diffraction by an incident, isotropic, cylindrical wave. This approximation of the non-isotropic, singly diffracted wave as an isotropic wave results in the type of above mentioned limitation. The inaccuracy which results from this approximation occurs mainly in the regions near the shadow boundary of the incident cylindrical wave.

Ryan and Rudduck<sup>2</sup> have obtained the radiation pattern of parallel-plate waveguides with arbitrary geometry by including only the single and double diffraction contributions. Yu and Rudduck<sup>3</sup> have included the third order diffraction contribution and subsequently employed a self-consistent method which includes all higher orders of diffraction from each edge. The

radiation pattern obtained by the above analyses have been found to be satisfactory in general. However, they do not describe the pattern adequately in the region  $60^\circ < \theta < 120^\circ$  where  $\theta$  is defined in Fig. 1.

In this analysis a surface integration technique will be employed in conjunction with wedge diffraction theory to improve the radiation pattern in this region. The formulation of the surface integral is presented in Chapter II. The validity of this formulation is tested on an isolated half-plane in Chapter III. Then the radiation pattern of a parallel-plate waveguide is obtained in Chapter IV using this formulation.

CHAPTER II  
FORMULATION OF HALF-SPACE RADIATION  
IN TERMS OF SURFACE INTEGRAL

In this chapter the radiation into the half-space  $y > 0$  is expressed in terms of the fields on the planar surface  $y = 0$  as shown in Fig. 2. Since the two dimensional problem in which the fields are independent of  $z$  is only of interest, the radiation can be expressed in terms of the fields on the  $x$ -axis. Only the TM case is considered, i. e., the magnetic field is  $z$ -polarized.

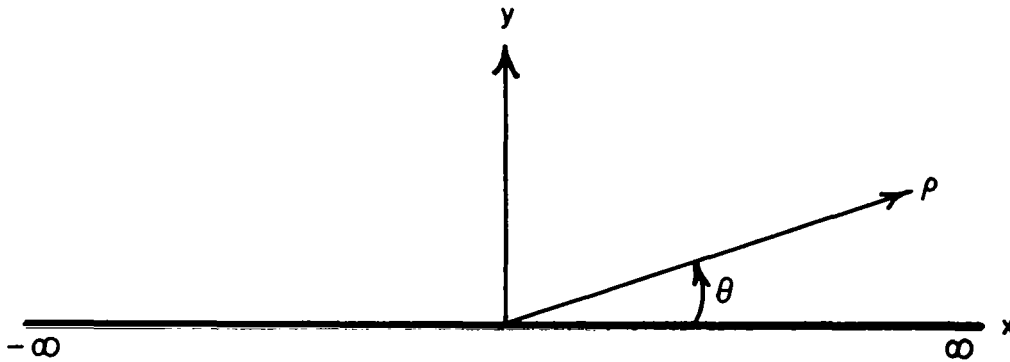


Fig. 2. Geometry of half-space radiation problem.

The field  $H_z$  satisfies the wave equation in the region  $y > 0$

$$(1) \quad (\nabla^2 + k^2) H_z = 0$$

where  $k = \frac{2\pi}{\lambda}$  is the free space propagation constant. The magnetic

field may be expressed in terms of the free space Green's function  $G_0$ , as

$$(2) \quad H_z = - \int_{-\infty}^{\infty} G_0 \left. \frac{\partial H_z(x', y')}{\partial y'} \right|_{y'=0} - H_z(x', 0) \left. \frac{\partial G_0}{\partial y'} \right|_{y'=0} dx'$$

where the prime sign (') denotes the source coordinates. Two choices of boundary conditions of the Green's function at  $y' = 0$  are possible for this half-space geometry. These are

$$(3) \quad G_0(x, y; x', 0) = 0$$

or

$$(4) \quad \left. \frac{\partial G_0(x, y; x', y')}{\partial y'} \right|_{y'=0} = 0$$

Using either Eq. (3) or Eq. (4), the expression for the magnetic field  $H_z$ , is given by either Eq. (5) or Eq. (6), respectively,

$$(5) \quad H_z = 2 \int_{-\infty}^{\infty} H_z(x', 0) \left. \frac{\partial G_0}{\partial y'} \right|_{y'=0} dx'$$

$$(6) \quad H_z = -2 \int_{-\infty}^{\infty} G_0 \left. \frac{\partial H_z(x', y')}{\partial y'} \right|_{y'=0} dx'$$

Using the asymptotic form of the free space Green's function, valid for large values of  $\rho$  in the polar coordinate, and the appropriate far field approximations, it can be shown that

$$(7) \quad G_0 \sim \frac{e^{-j\left(k\rho + \frac{\pi}{4}\right)}}{\sqrt{8\pi k\rho}} e^{+jkx' \cos \theta}$$

$$(8) \quad \left. \frac{\partial G_0}{\partial y'} \right|_{y'=0} \sim jk \sin \theta G_0$$

where  $\rho = (x^2 + y^2)^{\frac{1}{2}}$  and  $\theta = \tan^{-1} \frac{y}{x}$ .

Substituting Eq. (7) into Eq. (6) and Eq. (8) into Eq. (5), and suppressing the factor  $\frac{e^{-j\left(k\rho + \frac{\pi}{4}\right)}}{\sqrt{2\pi k\rho}}$ , the angular variation, or radiation pattern, is given by

$$(9) \quad R_Z(\theta) = - \int_{-\infty}^{\infty} \left. \frac{\partial H_Z(x', y')}{\partial y'} \right|_{y'=0} e^{+jkx' \cos \theta} dx',$$

or

$$(10) \quad R_Z(\theta) = \int_{-\infty}^{\infty} jk \sin \theta H_Z(x', 0) e^{+jkx' \cos \theta} dx'.$$

Thus, if either the magnetic field  $H(x', 0)$ , or its normal derivative i. e., tangential electric field  $E(x', 0)$ , is known on the surface ( $x'$ -axis), the far field radiation pattern can be evaluated.

A combination of the equivalence principle and the image theory can also be employed to derive Eqs. (9) and (10). This can be done by evaluating the equivalent magnetic and electric currents for the tangential fields on the surface. By use of image theory for this half-space geometry,<sup>5</sup> the radiation into  $y > 0$  can then be obtained from either twice the equivalent electric current or twice the equivalent magnetic current.

CHAPTER III  
PLANE WAVE DIFFRACTION  
BY A HALF-PLANE

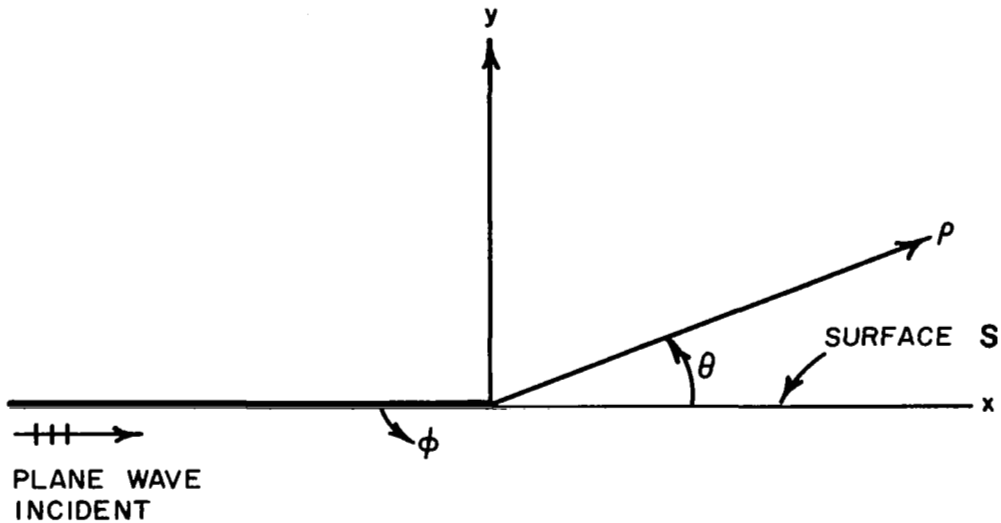


Fig. 3. Plane wave diffraction  
by a half-plane.

In this chapter the relationship is shown between the surface integral formulation, for plane wave diffraction by a half-plane, and the exact solution. In the comparison process several relationships are derived which are employed in subsequent chapters.

A. Half-Plane Diffraction  
Formulation

The problem of straight edge diffraction by a perfectly conducting half-plane was first solved by Sommerfeld.<sup>6</sup> For grazing incidence of a plane wave with its magnetic field polarized in the

z direction, the total field in the geometrical optics shadow region ( $0 < \theta < \pi$ ), as shown in Fig. 3, is given by

$$(11) \quad H_z(\rho, \pi+\theta) = V_B(\rho, \pi+\theta, 2) .$$

The incident wave is normalized to have unit-amplitude,<sup>1</sup> and the wedge diffraction function  $V_B(\rho, \phi, n)$  for a wedge of angle  $(2-n)\pi$  is discussed in Appendix A. For a half-plane (i. e.,  $n = 2$ ), the function  $V_B(\rho, \phi, 2)$  is given by

$$(12) \quad V_B(\rho, \phi, 2) = \frac{e^{-j\frac{\pi}{4}}}{\sqrt{\pi}} \left( \frac{-|\cos \frac{\phi}{2}|}{\cos \frac{\phi}{2}} \right) e^{jk\rho \cos \phi} \times \\ \int_{\sqrt{ak\rho}}^{\infty} e^{-j\tau^2} d\tau ,$$

where  $a = 1 + \cos \phi$ .

For large values of  $k\rho(1 + \cos \phi)$ , Eq. (12) may be asymptotically approximated as

$$(13) \quad V_B(\rho, \phi, 2) \sim \frac{-e^{-j(k\rho + \frac{\pi}{4})}}{2\sqrt{2\pi k\rho} \cos \frac{\phi}{2}}$$

Therefore, the magnetic field for the radiated wave in the region ( $0 < \theta < \pi$ ) is given by

$$(14) \quad H_z(\rho, \theta) = \frac{e^{-j(k\rho + \frac{\pi}{4})}}{\sqrt{2\pi k\rho}} \frac{1}{2 \sin \frac{\theta}{2}}$$

It is evident from Eq. (14) that the radiated wave appears to be a directional cylindrical wave radiating from the edge of the half-plane. Since only angular variations are of interest the factor  $\frac{e^{-j(k\rho + \frac{\pi}{4})}}{\sqrt{2\pi k\rho}}$  is suppressed. This gives the following radiation pattern function

$$(15) \quad R_z(\theta) = \frac{1}{2 \sin \frac{\theta}{2}} \cdot$$

### B. Surface Integral Representation

The surface integral representation of the far-field radiation pattern as shown in Eqs. (9) and (10) can be evaluated if the field is known on the surface S. For plane wave diffraction by a half-plane, the diffracted field and its normal derivative on the surface S ( $y=0$ ) are given by

$$(16) \quad H_z(x', 0) = \begin{cases} V_B(x', \pi^+, 2) = \frac{1}{2} e^{-jkx'} & (x' \geq 0), \\ V_B(x', 2\pi, 2) = \frac{e^{-j\frac{\pi}{4}}}{\sqrt{\pi}} e^{-jk|x'|} \int_0^\infty \frac{e^{-j\tau^2}}{\sqrt{2k|x'|}} d\tau & (x' \leq 0) \end{cases}$$

and

$$\begin{aligned}
(17) \quad \left. \frac{\partial H_z(x', y')}{\partial y'} \right|_{y'=0} &= \lim_{\phi' \rightarrow \pi^+} - \left( \sin \phi \frac{\partial V_B(\rho', \phi', 2)}{\partial \rho'} \right. \\
&\quad \left. + \frac{1}{\rho'} \cos \phi' \frac{\partial V_B(\rho', \phi', 2)}{\partial \phi'} \right) \\
&= \begin{cases} \frac{-e^{j\frac{\pi}{4}} e^{-jkx'}}{\sqrt{x'}} & (x' > 0) \\ 0 & (x' < 0) \end{cases} .
\end{aligned}$$

The integral for the radiation pattern which is obtained by substituting Eq. (17) into Eq. (9) can be analytically evaluated, giving

$$\begin{aligned}
(18) \quad R_z(\theta) &= 2 \int_0^\infty e^{j\frac{\pi}{4}} \frac{e^{-jkx'(1-\cos \theta)}}{\sqrt{x'}} dx' \\
&= \frac{2 e^{j\frac{\pi}{4}}}{\sqrt{2\pi(1-\cos \theta)}} \int_0^\infty \frac{e^{-ju}}{\sqrt{u}} du \\
&= \frac{1}{2 \sin \frac{\theta}{2}}
\end{aligned}$$

Comparing Eq. (18) with Eq. (15) it is seen that the radiation pattern function in the shadow region  $0 < \theta < \pi$ , as obtained by the surface integration technique, is of course, exactly equal to the exact solution.

From the other boundary condition on the Green's function as shown in Eq. (3), the integral representation of the pattern function can be derived by substituting Eq. (16) into Eq. (10), giving

$$(19) \quad R_z(\theta) = jk \sin \theta \int_0^{\infty} \frac{1}{2} e^{-jkx'(1-\cos \theta)} dx' \\ + jk \sin \theta \int_{-\infty}^0 e^{+jkx' \cos \theta} V_B(x', 2\pi, 2) dx' .$$

The value of the first integral in Eq. (19) can be analytically evaluated by means of a distributions or generalized function,<sup>7</sup> giving

$$(20) \quad \frac{jk \sin \theta}{2} \int_0^{\infty} e^{-jkx'(1-\cos \theta)} dx' \\ = \frac{jk \sin \theta \pi \delta(k(1-\cos \theta))}{2} + \frac{\sin \theta}{2(1-\cos \theta)} .$$

The second term in Eq. (19) can be simplified by interchanging the limits of integration obtaining,

$$(21) \quad jk \sin \theta \int_0^{\infty} e^{-jkx' \cos \theta} V_B(x', 2\pi, 2) dx'$$

For values of  $x'$  greater than some value  $x_m$ , the function  $V_B(x', 2\pi, 2)$  in Eq. (21) can be approximated by the asymptotic

expression given in Eq. (13). Thus, Eq. (21) can be written

$$(22) \quad jk \sin \theta \int_0^{x_m} e^{-jkx' \cos \theta} V_B(x', 2\pi, 2) dx' \\ + jk \sin \theta \int_{x_m}^{\infty} \frac{e^{-j\frac{\pi}{4}} e^{-jkx'(1+\cos \theta)}}{2\sqrt{2\pi kx'}} dx'$$

The first term is numerically evaluated by computer. The second term can be analytically evaluated in terms of the Fresnel integral which is defined as

$$(23) \quad F(x) = \frac{1}{\sqrt{2\pi}} \int_x^{\infty} \frac{e^{-jt}}{\sqrt{t}} dt \\ = \sqrt{\frac{2}{\pi}} \int_{\sqrt{x}}^{\infty} e^{-ju^2} du$$

where

$$F(0) = 0.5 \sqrt{2} e^{-j\frac{\pi}{4}}$$

$$F(\infty) = 0$$

Consequently, the second term in Eq. (22) is given by

$$(24) \quad \frac{k \sin \theta}{2\sqrt{2\pi k}} e^{+j\frac{\pi}{4}} \int_{x_m}^{\infty} \frac{e^{-jkx'(1+\cos \theta)}}{\sqrt{x'}} dx' \\ = \frac{\sin \theta}{2\sqrt{1+\cos \theta}} e^{j\frac{\pi}{4}} \int_{kx_m(1+\cos \theta)}^{\infty} \frac{e^{-jt}}{\sqrt{2\pi t}} dt \\ = \frac{\sin \theta}{2\sqrt{1+\cos \theta}} e^{j\frac{\pi}{4}} F(kx_m(1+\cos \theta)) .$$

This Fresnel integral will be employed frequently in the next chapter to evaluate integrals which decay as  $x^{-\frac{1}{2}}$ .

Using Eqs. (20) to (24), the radiation pattern function in the shadow region ( $0 < \theta < \pi$ ) as indicated in Eq. (19), can be written as

$$(25) \quad R_z(\theta) = \frac{\sin \theta}{2(1 - \cos \theta)} + jk \sin \theta \int_0^{x_m} e^{-jkx' \cos \theta} V_B(x', 2\pi, 2) dx' \\ + \frac{\sin \theta}{2\sqrt{1 + \cos \theta}} e^{+j\frac{\pi}{4}} F(kx_m(1 + \cos \theta))$$

Numerical results have been computed from Eq. (25) for values of  $x_m$  ranging from two to ten wavelengths and for several values of the angle theta as shown in Table I. Accuracies of about 0.5% are obtained by the numerical evaluation as compared with the exact solution in Eq. (15). Thus, we can conclude that this method of calculating the radiation pattern is satisfactory.

TABLE I

Theta in Degrees	$1/(2 \sin \frac{\theta}{2})$	$x_m$ in $\lambda$		
		2	5	10
70	0.87172	0.87199	0.87141	0.87125
80	0.77786	0.77610	0.77642	0.77646
90	0.70711	0.70598	0.70640	0.70654
100	0.65270	-	-	0.65215

This evaluation of the diffracted fields from a half-plane illustrates a method for evaluating the surface integral for which the fields on surface  $S$  decay as  $x^{-\frac{1}{2}}$  and indicates the accuracy of the numerical evaluation. Since computer evaluation for  $0 < x' < x_m$  is expensive, it is desirable to use as small a value for  $x_m$  as practical.

CHAPTER IV  
THE RADIATION PATTERN OF A TEM MODE  
PARALLEL-PLATE WAVEGUIDE

In this chapter the radiation pattern of the parallel-plate waveguide, shown in Fig. 1, is analyzed by the surface integration technique discussed in the previous chapters. The parallel-plate waveguide for this problem is formed from two half-planes separated by a guide width  $h$ , and aligned for a normal truncation angle.

The TEM mode radiation pattern, due to an incident plane wave propagating parallel to the axis of the guide, with the electric field polarized perpendicular to the guide walls, is analyzed in the following paragraph. The exact solution for this particular geometry has been obtained by the Weiner-Hopf technique as given in Appendix B.

Because of the symmetrical excitation and geometry, the pattern is symmetrical with respect to the angle  $\theta$ . Thus, the pattern is calculated only in the region  $0 < \theta < \pi$  and consequently, the surface of integration is chosen to correspond to the  $x$ -axis. (However, if the pattern is chosen in the region  $-\pi < \theta < 0$ , the surface  $S$  corresponds to  $y = -h$ .)

The radiation pattern can be calculated using the Green's function with either one of its boundary conditions (Eqs. (9) and (10)). However, in the following development, only Eq. (10) will be

employed, which is rewritten for convenience,

$$(10) \quad R_z(\theta) = \int_{-\infty}^{\infty} jk \sin \theta H_z(x', 0) e^{jkx' \cos \theta} dx' .$$

The magnetic fields  $H_z(x', 0)$ , on the surface  $S$ , are calculated by the theory of wedge diffraction.<sup>1</sup> Three terms of the surface field distributions will be considered.

The first term to contribute to the pattern consists of the diffracted fields (A, B, C) on the surface  $S$ , as shown in Fig. 4.

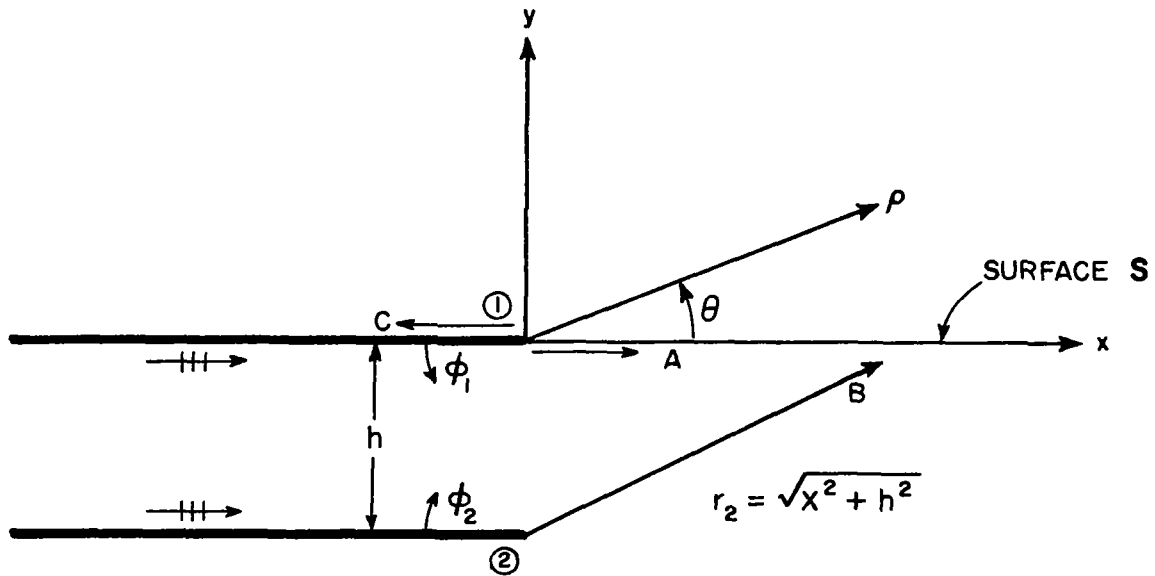


Fig. 4. First term (singly diffracted waves from both edges).

These fields are those of the plane wave diffraction by the isolated half-planes:

$$(26) \quad A: H_1^{(1)}(x', 0) = \frac{1}{2} e^{-jkx'} \quad (x' > 0)$$

$$(27) \quad B: H_2^{(1)}(x', 0) = V_B(r_2, \phi_2, 2) \quad (x' > 0)$$

where

$$r_2 = \sqrt{h^2 + x'^2} \quad \phi_2 = \frac{\pi}{2} + \tan^{-1} \frac{x'}{h}$$

and

$$(28) \quad C: H_1^{(1)}(x', 0) = V_B(x', 2\pi, 2) \quad (x' < 0)$$

The subscript 1, 2 denotes edges (1) and (2) respectively and the superscript (1) denotes the first order diffraction due to the incident plane wave.

It is noted that the singly diffracted field on the upper surface  $S$  ( $x \geq 0$ ) is proportional to  $x'^{-\frac{1}{2}}$  for values of  $x'$  greater than some value  $x_m$ . It can be shown that the sum of Eqs. (26) and (27) for  $x' \geq x_m$  is approximately given by

$$(29) \quad H_1^{(1)}(x', 0) + H_2^{(1)}(x', 0) \approx \frac{e^{j\frac{\pi}{4}} \sqrt{k} a}{\sqrt{2\pi}} \frac{e^{-jkx'}}{\sqrt{x'}}$$

The singly diffracted field on the lower surface  $S$  ( $x' \leq 0$ ) is that of the isolated half-plane as discussed in the previous chapter.

The radiation pattern function  $R_{z1}(\theta)$ , due to the singly diffracted fields on the surface S, can be expressed in terms of (1) numerical integration over a finite portion of the surface and (2) the Fresnel integral which represents the integration over the remainder of the surface (the same technique was used in Chapter III) giving

$$\begin{aligned}
 (30) \quad R_{z1}(\theta) = & \frac{\sin \theta}{2\sqrt{1 + \cos \theta}} e^{j\frac{\pi}{4}} F(kx_m(1 + \cos \theta)) \\
 & + \int_0^{x_m} jk \sin \theta e^{-jkx' \cos \theta} V_B(x', 2\pi, 2) dx' \\
 & + \int_0^{x_m} jk \sin \theta e^{+jkx' \cos \theta} \left[ \frac{1}{2} e^{-jkx'} + V_B(r_2, \phi_2, 2) \right] dx' \\
 & + \frac{ka \sin \theta e^{+j\frac{3\pi}{4}}}{\sqrt{1 - \cos \theta}} F(kx_m(1 - \cos \theta))
 \end{aligned}$$

The first two terms in Eq. (30) correspond to the lower surface integration obtained from Eq. (22) whereas the last two terms represent the upper surface integration.

The next two contributions to the radiation pattern take into account fields on the surface S, which result from interactions between the half-planes. The second term to contribute to the pattern function  $R_{z2}(\theta)$  consists of the doubly diffracted fields on the surface S from edge (1) which resulted from the singly diffracted wave from edge (2). The doubly diffracted fields are analyzed by

the wedge diffraction method.<sup>1</sup> By this method the singly diffracted wave from edge (2) is approximated by a uniform cylindrical wave in order to analyze the doubly diffracted wave from edge (1). Thus, the effective source for the singly diffracted wave is a line source located at edge (2) as shown in Fig. 5.

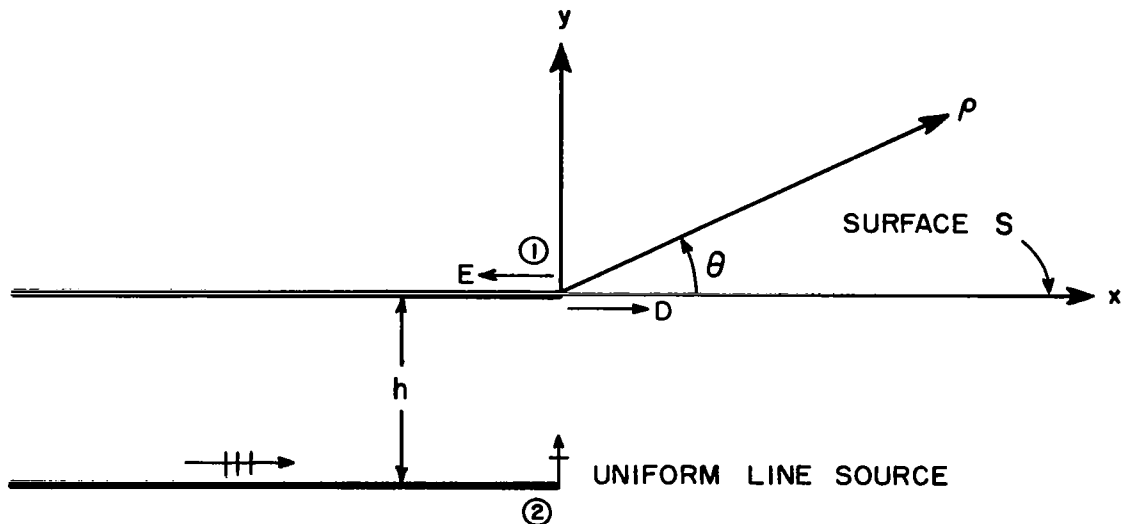


Fig. 5. Second term (doubly diffracted wave from edge (1)).

The approximation by an isotropic line source is apparent by examining the plane wave diffracted field in the direction as shown in Fig. 5.

$$(31) \quad V_B(\rho, 90^\circ, 2) \sim \frac{e^{-jk\rho}}{\sqrt{\rho}} \left( \frac{-e^{-j\frac{\pi}{4}}}{\sqrt{4\pi k}} \right)$$

Therefore, the amplitude of the line source located at edge (2) is  $-e^{-j\frac{\pi}{4}} / \sqrt{4\pi k}$ . The doubly diffracted field from edge (1) at the surface S,

is obtained by application of cylindrical wave diffraction (see Appendix A) and is given by

$$\begin{aligned}
 (32) \quad \begin{matrix} \text{D:} \\ \text{E:} \end{matrix} \quad H_1^{(2)}(x', 0) &= \frac{-e^{-j\frac{\pi}{4}}}{\sqrt{4\pi k}} \frac{e^{-jk(h+|x'|)}}{\sqrt{h+|x'|}} e^{jk\frac{h|x'|}{h+|x'|}} \\
 &\times \left[ V_B\left(\frac{h|x'|}{h+|x'|}, 90^\circ, 2\right) + V_B\left(\frac{h|x'|}{h+|x'|}, 270^\circ, 2\right) \right] \\
 &= \begin{cases} 0 & (x' > 0) \\ \frac{-e^{-j\frac{\pi}{4}}}{\sqrt{\pi k}} \frac{e^{-jk(h+|x'|)}}{\sqrt{h+|x'|}} e^{jk\frac{h|x'|}{h+|x'|}} V_B\left(\frac{h|x'|}{h+|x'|}, 270^\circ, 2\right) & (x' < 0) \end{cases}
 \end{aligned}$$

where the superscript (2) corresponds to second order diffraction.

The assumption of uniform cylindrical wave incidence, in the previous applications of the wedge diffraction theory, does not accurately give the radiated fields in the region near  $\theta = 90^\circ$  as will be shown later. The surface integration technique improves the accuracy in this region since it includes the effect of the non-isotropic nature of the wave from edge (2).

For  $|x'|$  greater than some value of  $x_m$  the doubly diffracted field in Eq. (32) can be asymptotically approximated by

$$(33) \quad H_1^{(2)}(x', 0) \sim \frac{-e^{-j\frac{\pi}{4}}}{\sqrt{\pi k}} \frac{e^{-jk|x'|}}{\sqrt{|x'|}} V_B(h, 270^\circ, 2) \quad (x' < 0)$$

It is noted that  $V_B(h, 270^\circ, 2)$  is a constant, thus the diffracted fields in Eq. (33) is proportional to  $|x'|^{-\frac{1}{2}}$ . Thus, the contribution of the doubly diffracted field from edge (1) on the surface S, to the pattern function  $R_{zz}(\theta)$ , is given by

$$(34) \quad R_{zz}(\theta) = \frac{-\sqrt{2} e^{j\frac{\pi}{4}} \sin \theta}{\sqrt{1 + \cos \theta}} V_B(h, 270^\circ, 2) F(kx_m(1 + \cos \theta)) \\ + \frac{-e^{j\frac{\pi}{4}} \sqrt{k} \sin \theta}{\sqrt{\pi}} \int_0^{x_m} \frac{e^{-jk(h+x')}}{\sqrt{h+x'}} e^{jk \frac{hx'}{h+x'}} e^{-jkx' \cos \theta} \\ \times V_B\left(\frac{hx'}{h+x'}, 270^\circ, 2\right) dx'$$

The third term to contribute to the pattern consists of the doubly diffracted fields from edge (2) on the surface S. These fields are calculated in the same way as the doubly diffracted fields from edge (1). In this case, the singly diffracted wave from edge (1) is represented by an isotropic line source at edge (1). The doubly diffracted fields on the surface, S, from edge (2) result from the diffraction of the uniform wave from this equivalent line source as shown in Fig. 6. The doubly diffracted field from edge (2) is given by

$$(35) \quad H_2^{(2)}(x', 0) = \frac{-e^{-j\frac{\pi}{4}}}{\sqrt{4\pi k}} \frac{e^{-jk(h+r_2)}}{\sqrt{h+r_2}} e^{jk \frac{hr_2}{h+r_2}} \\ \times \left\{ V_B\left(\frac{hr_2}{h+r_2}, \alpha_2, 2\right) + V_B\left(\frac{hr_2}{h+r_2}, \pi + \alpha_2, 2\right) \right\}$$

where

$$r_2 = \sqrt{h^2 + x'^2}$$

$$\alpha_2 = \tan^{-1} \frac{x'}{h}$$

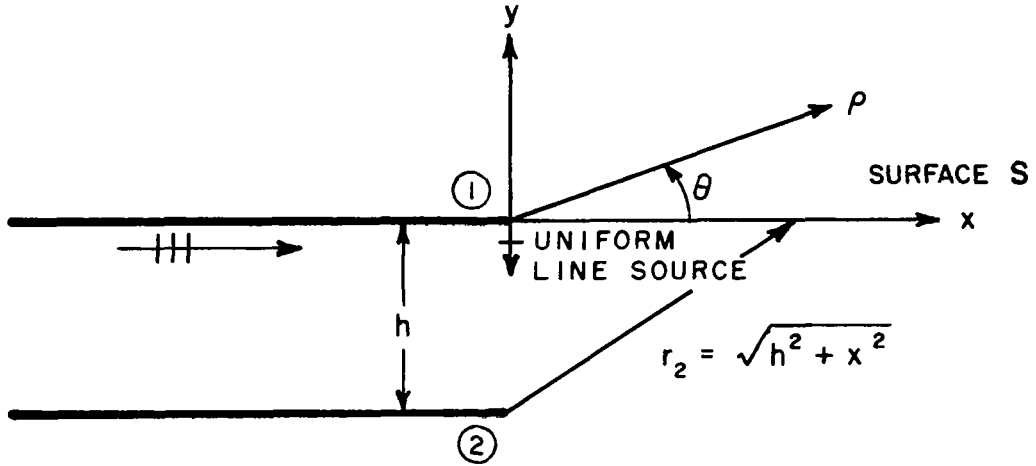


Fig. 6. Third term (doubly diffracted wave from edge (2)).

For large values of  $x'$ , the sum of the two  $V_B$  functions is extremely small. Therefore,  $H_2^{(2)}(x', 0)$  is assumed negligible for  $x$  greater than some value  $x_m$ .

Thus, the contribution to the radiation pattern function  $R_{z3}(\theta)$ , due to the doubly diffracted field from edge (2), is given by

$$(36) \quad R_{z3}(\theta) = -k \sin \theta \frac{e^{+j\frac{\pi}{4}}}{\sqrt{4\pi k}} \int_0^{x_m} \frac{e^{-jk(h+r_2)}}{\sqrt{h+r_2}} e^{jk\frac{hr_2}{h+r_2}} e^{+jkx' \cos \theta} \\ \times \left[ V_B\left(\frac{hr_2}{h+r_2}, \alpha_2, 2\right) + V_B\left(\frac{hr_2}{h+r_2}, \pi + \alpha_2, 2\right) \right] dx'$$

TABLE II

The pattern function  $R_z(\theta) = \int_{-\infty}^{\infty} jk \sin \theta e^{jkx' \cos \theta} H_z(x' 0) dx'$

Surface Integration	Lower Part		Upper Part	
	$-\infty \leq x' \leq -x_m$	$-x_m \leq x' \leq 0$	$0 \leq x' \leq x_m$	$x_m \leq x' \leq \infty$
First Term $R_{z1}(\theta)$	$\frac{\sin \theta}{2\sqrt{1+\cos \theta}} e^{j\frac{\pi}{4}} F(kx_m(1+\cos \theta))$	$\int_0^{x_m} jk \sin \theta e^{-jkx' \cos \theta} V_B(x', 2\pi, 2) dx'$	$\int_0^{x_m} jk \sin \theta e^{+jkx' \cos \theta} \times [\frac{1}{2}e^{-jkr'} + V_B(r_2\phi_2, 2)] dx'$	$\frac{ka \sin \theta e^{+j\frac{3\pi}{4}}}{\sqrt{1-\cos \theta}} \times F(kx_m(1-\cos \theta))$
Second Term $R_{z2}(\theta)$	$-\frac{\sqrt{2} e^{+j\frac{\pi}{4}} \sin \theta}{\sqrt{1+\cos \theta}} V_B(h, 270^\circ, 2) \times F(kx_m(1+\cos \theta))$	$-e^{j\frac{\pi}{4}} \frac{k \sin \theta}{\sqrt{\pi k}} \int_0^{x_m} \frac{e^{-jk(h+x')}}{\sqrt{h+x'}} e^{-jkx' \cos \theta} e^{\frac{khx'}{j(h+x')}} V_B\left(\frac{hx'}{h+x'}, 270^\circ, 2\right) dx'$		
Third Term $R_{z3}(\theta)$			$-e^{j\frac{\pi}{4}} \frac{k \sin \theta}{\sqrt{4\pi k}} \int_0^{x_m} \frac{e^{jk(h+r_2)}}{\sqrt{h+r_2}} e^{jkx' \cos \theta} e^{\frac{jkhr_2}{h+r_2}} \times \left[ V_B\left(\frac{hr_2}{h+r_2}, \alpha_2, 2\right) + V_B\left(\frac{hr_2}{h+r_2}, \pi + \alpha_2, 2\right) \right] dx'$	

The radiation pattern function of the parallel-plate waveguide (Fig. 1) due to the three terms (Eqs. (30), (34) and (36)) are presented in Table II in the appropriate regions.

Both the magnitude and phase of the first two terms of the radiation pattern function, as given in Table II, were calculated for five values of guide width  $h$ , ranging from  $0.1$  to  $0.5\lambda$  as shown in Tables III to VII. The effect of the third term was included for guide width of  $0.1$ ,  $0.2$  and  $0.3\lambda$ . It can be seen that as the guide width increases the effect of the third term decreases.

The radiation pattern of the parallel-plate waveguide formulated by the Weiner Hopf technique is given in Appendix B and has its phase references to the center of the guide aperture. This phase reference was shifted to the edge of the guide so as to be the same as that in the surface integration technique.

The radiation patterns were plotted for these five values of guide width as shown in Figs. 7 to 11. It is noted that for guide widths of  $0.2$  and  $0.3\lambda$ , the values of the exact radiation pattern (Weiner Hopf technique) lies in between the surface integration pattern function with and without the third term contribution.

It is believed that the radiation pattern, including the contributions due to subsequent higher order interactions between the two edges, will be in between the two extremes computed with and without the third term contribution. The fields on the

surface  $S$ , due to the higher order interactions, will decrease as the guide width increases. The maximum error as compared with the exact solution is approximately five percent in magnitude and three degrees in phase for guide widths of  $0.2$  and  $0.3\lambda$ . The radiation pattern for guide widths of  $0.4$  and  $0.5\lambda$  are shown in Figs. 10 and 11, respectively.

The error is small as compared with the exact solution. It is noted that the radiation pattern formulated by the surface integration technique agrees well even for the guide width as small as  $0.1\lambda$  as shown in Fig. 7.

The radiation pattern as analyzed by the wedge diffraction method<sup>2</sup> is also given in Figs. 7 to 11, and in Tables III-VII. In the wedge diffraction method, the pattern is obtained directly from the sum of the singly and doubly diffracted rays in region  $y > 0$ . Based on the comparison, the improvement in accuracy of the surface integration technique is evident.

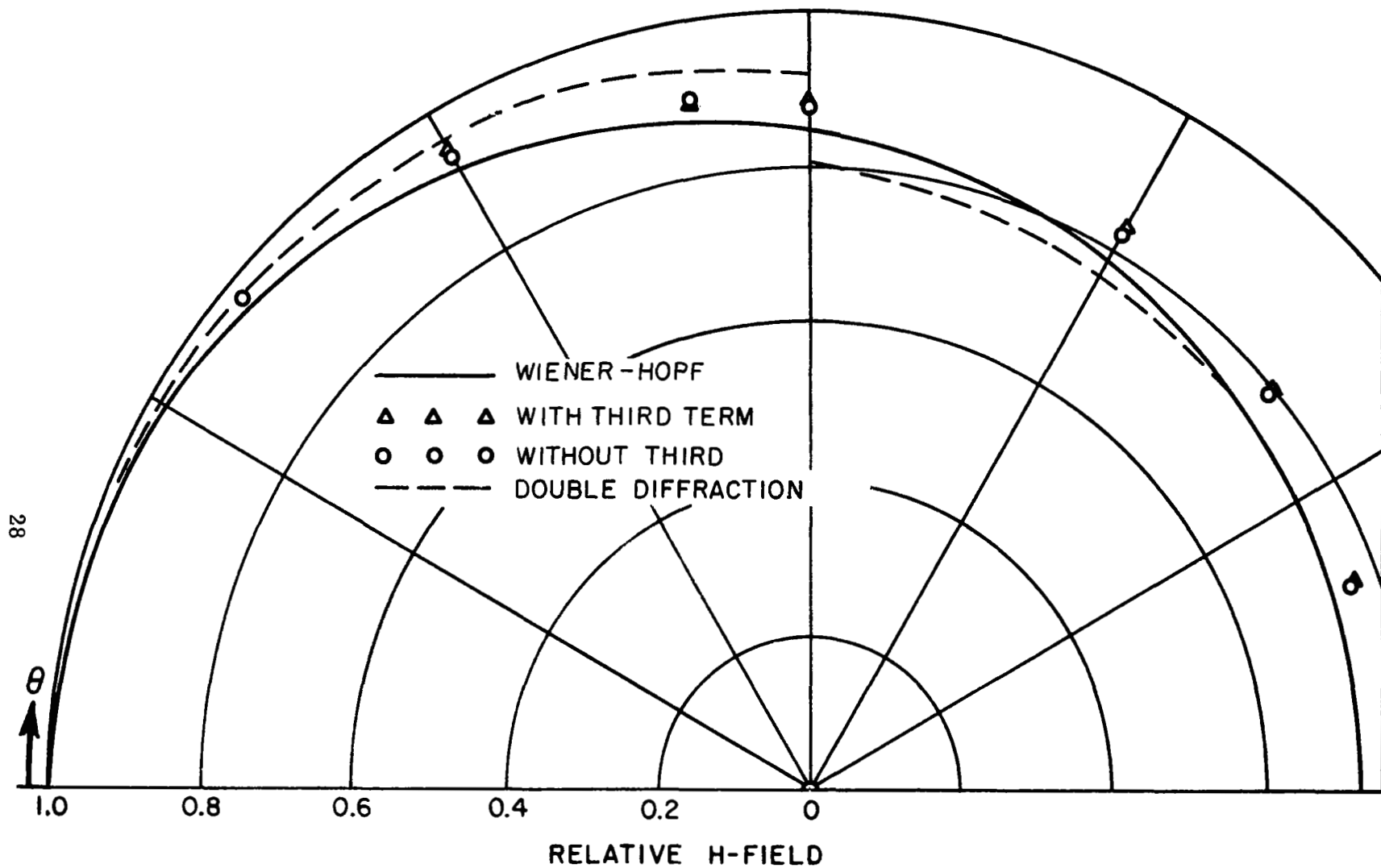


Fig. 7. Radiation pattern for TEM mode parallel-plate waveguide ( $h/\lambda = 0.1$ ).

TABLE III

Theta in Degrees	Weiner-Hopf		Double Diffraction		Surface Intergation			
	Mag	Phase	Mag	Phase	Without Third Term		With Third Term	
					Mag	Phase	Mag	Phase
1	1.0	89.7	1.0	89.7				
20	0.990	83.3	0.995	83.4				
40	0.961	76.4	0.982	76.8	0.972	72.8	0.973	76.7
60	0.919	69.8	0.964	71.3	0.938	65.6	0.942	70.0
80	0.871	63.0	0.938	68.2	0.898	59.7	0.905	64.1
90	0.848	61.4	0.800	44.3	0.878	57.3	0.886	61.5
120	0.785	55.4	0.763	47.5	0.823	52.1	0.831	55.3
140	0.755	52.9	0.748	47.6	0.792	50.1	0.798	52.3
160	0.737	51.3	0.738	47.3	0.763	48.8	0.767	50.0
180	0.730	50.9						

29

Guide Width  $0.1\lambda$

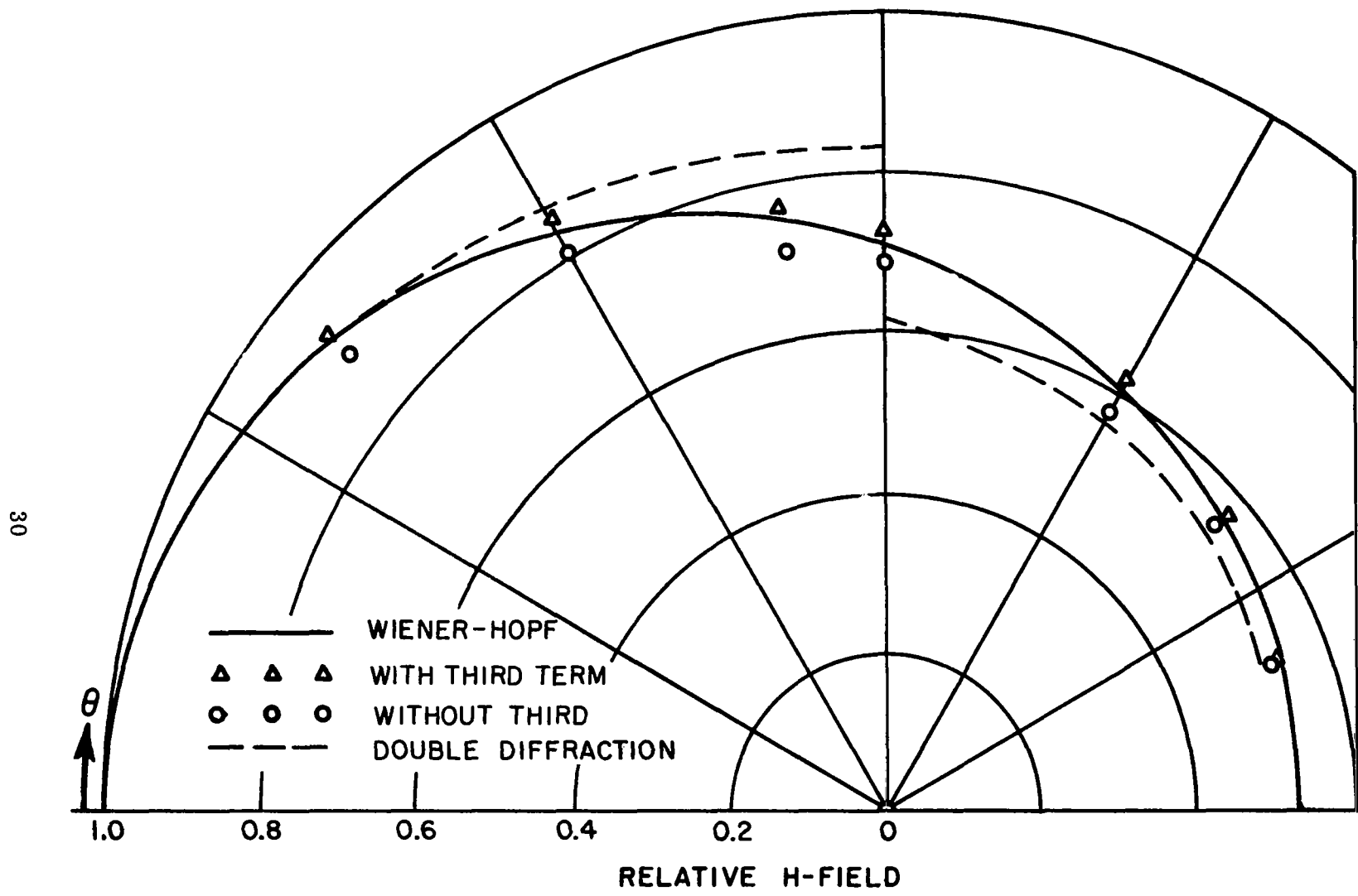


Fig. 8. Radiation pattern for TEM mode parallel plate waveguide ( $h/\lambda = 0.2$ ).

TABLE IV

Theta in Degrees	Weiner Hopf		Double Diffraction		Surface Diffraction			
	Mag	Phase	Mag	Phase	Without Third Term		With Third Term	
					Mag	Phase	Mag	Phase
1	1.0	89.4	1.0	89.4				
20	0.977	76.2	0.980	76.9				
40	0.916	64.7	0.929	63.5	0.891	63.7	0.930	65.2
60	0.834	53.6	0.871	51.3	0.805	52.6	0.848	54.1
80	0.747	44.5	0.833	42.0	0.720	43.7	0.761	45.0
90	0.706	40.9	0.619	35.3	0.682	40.1	0.720	41.4
100	0.670	37.7	0.599	34.2				
120	0.609	33.0	0.564	31.7	0.592	32.6	0.618	33.4
140	0.566	30.0	0.536	29.7	0.553	29.9	0.571	30.4
160	0.542	28.3	0.519	28.5	0.528	28.5	0.537	28.8
180	0.535	27.7						

Guide Width  $0.2\lambda$

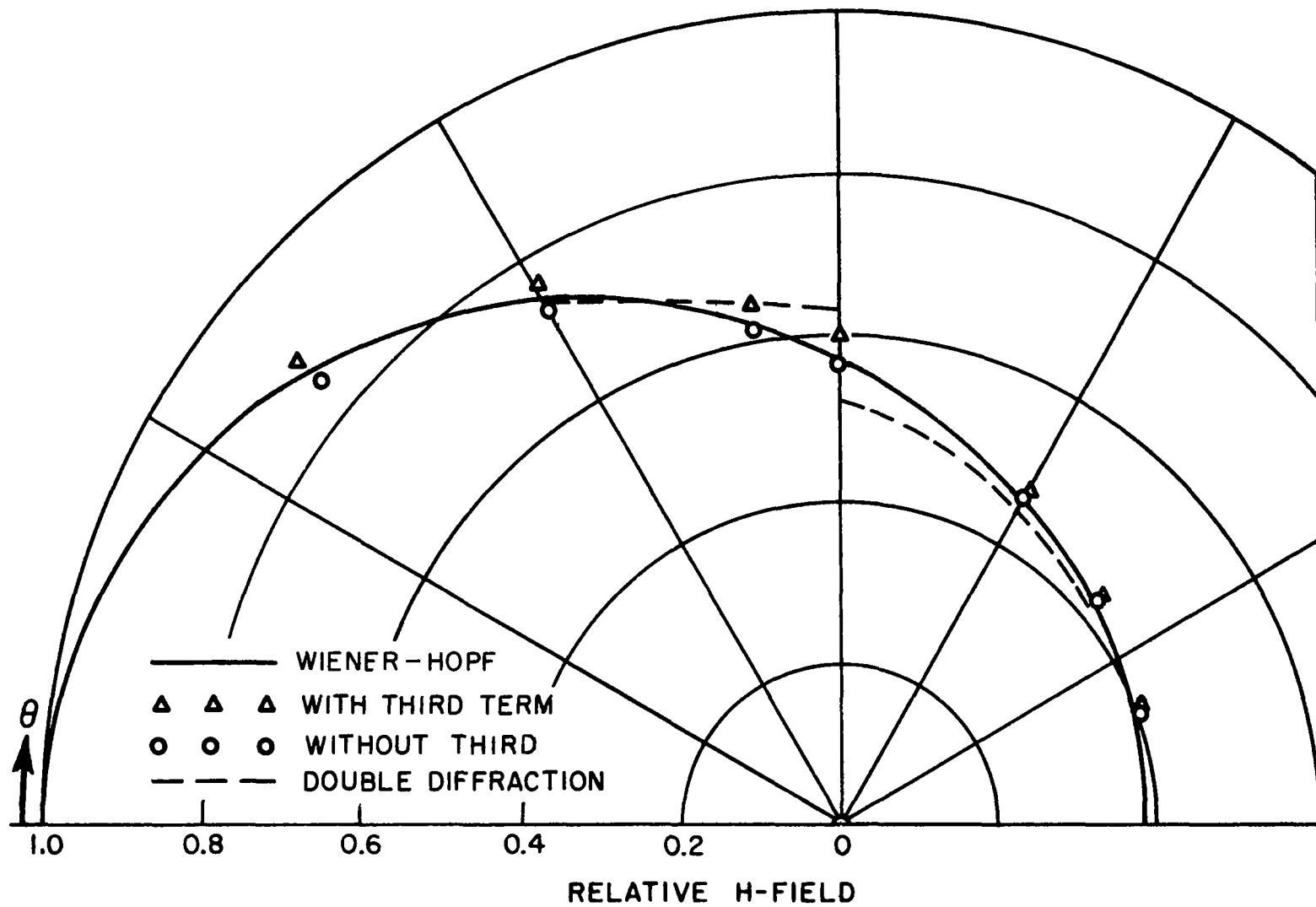


Fig. 9. Radiation pattern for TEM mode parallel plate waveguide ( $h/\lambda = 0.3$ ).

TABLE V

Theta in Degrees	Weiner Hopf		Double Diffraction		Surface Diffraction			
	Mag	Phase	Mag	Phase	Without Third Term		With Third Term	
					Mag	Phase	Mag	Phase
1	1.0	89.1	1.0	89.1				
20	0.964	71.1	0.961	70.9				
40	0.868	54.9	0.859	52.3	0.851	54.1	0.887	53.3
60	0.746	38.8	0.737	35.1	0.729	39.9	0.761	38.4
80	0.629	27.7	0.648	19.7	0.616	29.0	0.643	27.2
90	0.578	23.5	0.520	23.5	0.567	24.9	0.591	23.1
120	0.466	15.3	0.446	17.3	0.461	17.0	0.475	15.4
140	0.422	12.7	0.413	14.8	0.420	14.4	0.429	13.1
160	0.397	11.3	0.393	13.5	0.397	13.2	0.401	12.6
180	0.390	10.9	0.387					

33

Guide Width  $0.3\lambda$

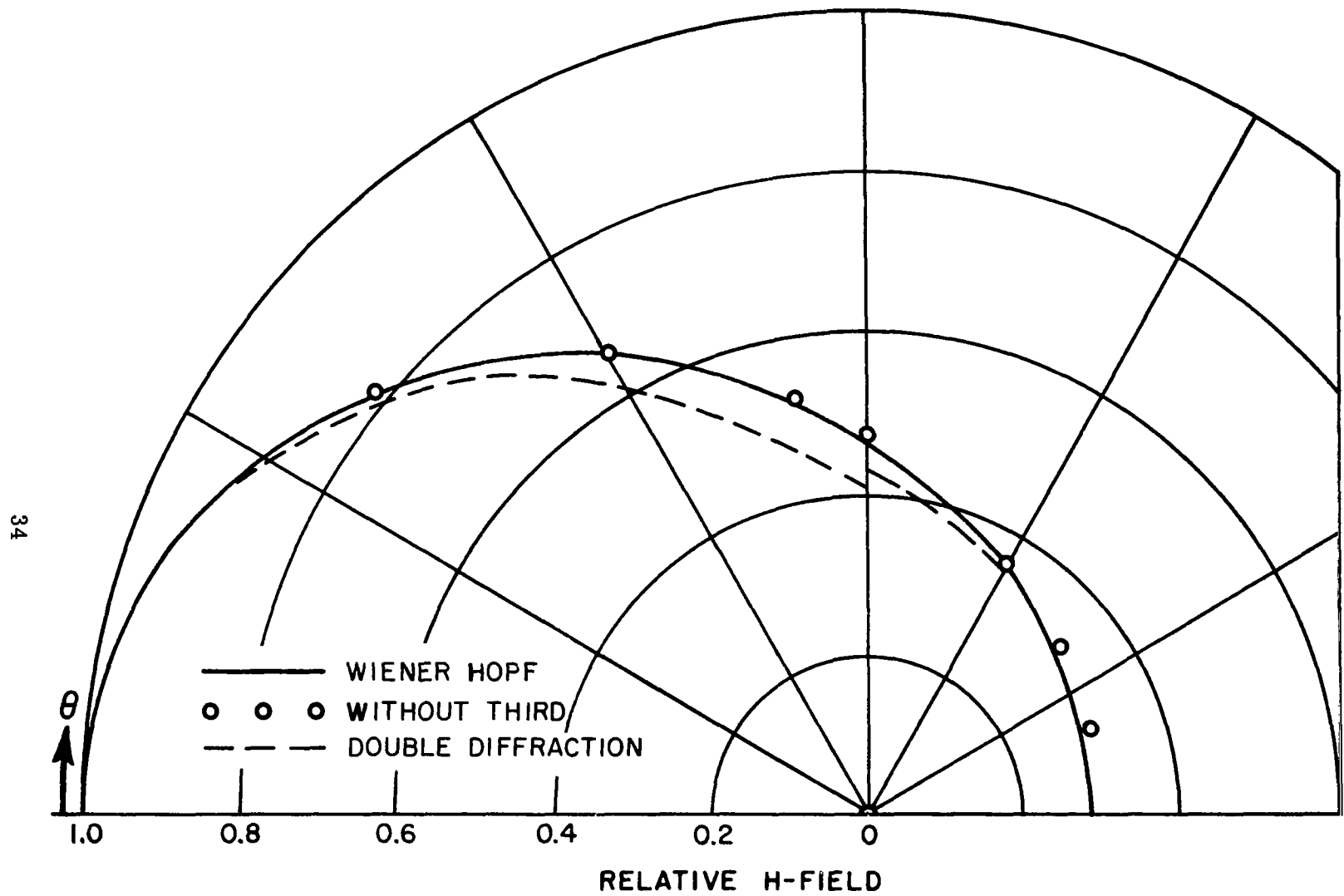


Fig. 10. Radiation pattern for TEM mode parallel plate waveguide ( $h/\lambda = 0.4$ ).

TABLE VI

Theta in Degrees	Weiner Hopf		Double Diffraction		Surface Integration			
	Mag	Phase	Mag	Phase	Without Third Term		With Third Term	
	Mag	Phase	Mag	Phase	Mag	Phase	Mag	Phase
1	1.0	88.7	1.0	88.7				
20	0.948	65.2	0.943	65.2				
40	0.817	42.8	0.797	42.5	0.815	43.8		
60	0.659	26.0	0.617	23.3	0.658	26.7		
80	0.520	12.5	0.463	5.3	0.529	14.2		
90	0.464	8.0	0.437	10.6	0.469	10.1		
120	0.352	2.2	0.353	3.6	0.360	2.8		
140	0.312	-0.6	0.318	1.4	0.321	0.7		
160	0.291	-1.4	0.299	0.3	0.300	-0.0		
180	0.284	-1.5						

Guide Width  $0.4\lambda$

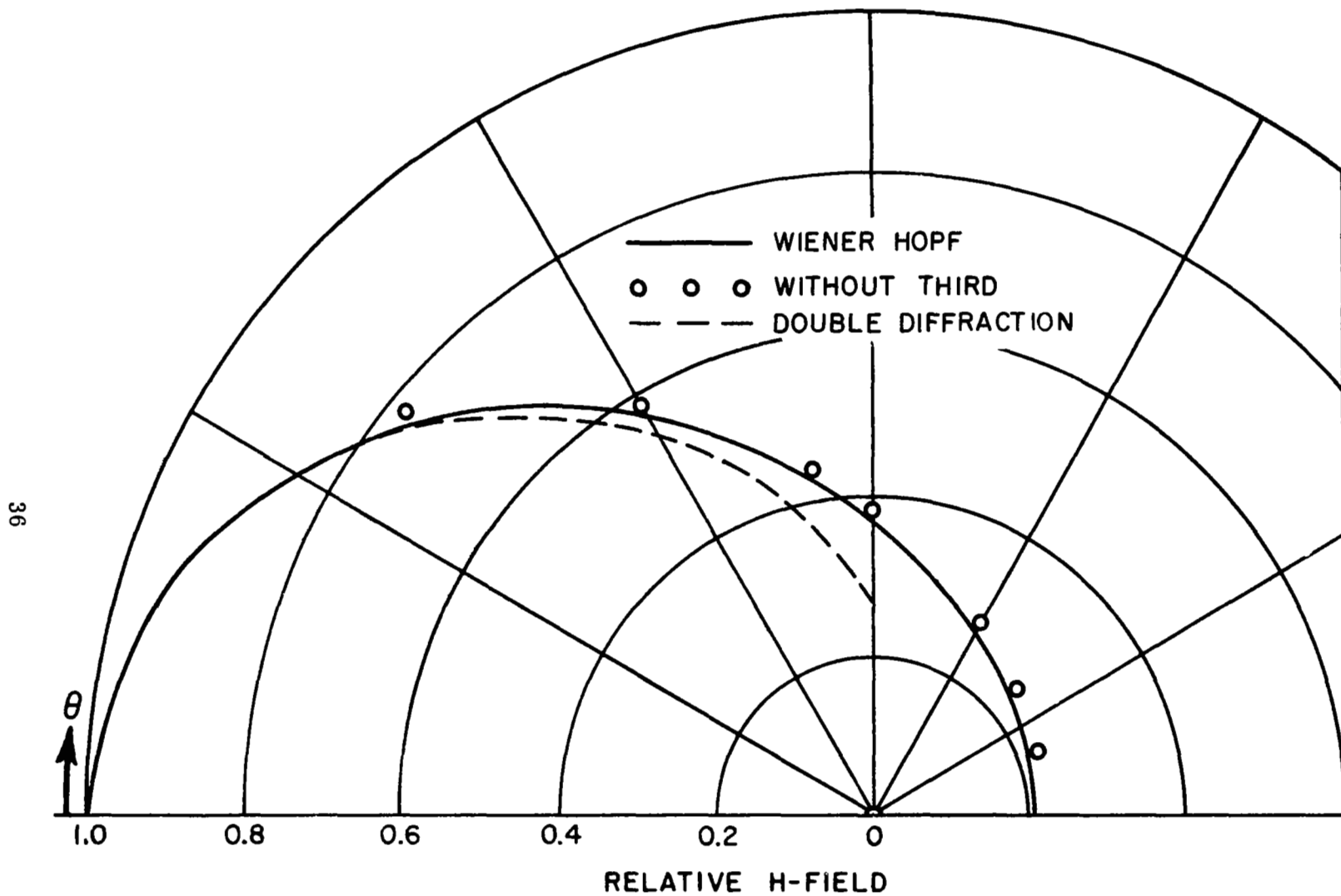


Fig. 11. Radiation pattern for TEM mode parallel plate waveguide ( $h/\lambda = 0.5$ ).

TABLE VII

Theta in Degrees	Weiner Hopf		Double Diffraction		Surface Integration			
	Mag	Phase	Mag	Phase	Without Third Term		With Third Term	
					Mag	Phase	Mag	Phase
1	1.0		1.0	88.4				
20	0.931		0.928	59.5				
40	0.762		0.748	33.2	0.774	33.0		
60	0.573		0.533	13.9	0.583	12.8		
80	0.420		0.346	0.9	0.435	-0.4		
90	0.364		0.357	-2.6	0.376	-4.5		
120	0.261		0.270	-9.0	0.272	-10.1		
140	0.229		0.239	-10.4	0.239	-11.2		
160	0.213		0.223	-10.9	0.223	-11.3		
180	0.209							

Guide Width  $0.5\lambda$

## CHAPTER V CONCLUSION

In this publication the radiation pattern of the thin-walled parallel-plate waveguide is analyzed by a surface integration method. This analysis gives an improvement in the accuracy of the pattern in the region near the plane of the guide aperture, as compared to conventional wedge diffraction analysis. The comparison is based on the exact solution given in Appendix B and which is valid for guide widths from 0 to  $0.5\lambda$ . The radiation pattern obtained by the surface integration analysis agrees quite well with the exact pattern for guide widths ranging from 0.1 to  $0.5\lambda$ . By the nature of the surface integration analysis, its accuracy increases with guide width.

The surface integration approach may be applied to other diffraction problems as a means of overcoming the limitations of the wedge diffraction method. Specifically the radiation pattern analysis presented here may be extended to other waveguide geometries, i. e., guides mounted in infinite ground planes and guides with arbitrary truncation angles.

## APPENDIX A

The two-dimensional problem of the electromagnetic field, in the neighborhood of a conducting wedge, illuminated by a plane wave, was first solved by Sommerfeld.<sup>6</sup> The solution for a half-plane (zero wedge angle) was formulated in terms of the Fresnel integral.

Subsequently, Pauli formulated the solution for wedges of arbitrary angles in which the dominant term is the Fresnel integral giving,

$$(37) \quad V_B(\rho, \phi, n) = \frac{2e^{j\frac{\pi}{4}}}{\sqrt{\pi}} \frac{1}{n} \sin \frac{\pi}{n} \frac{|\cos \frac{\phi}{2}|}{\cos \frac{\pi}{n} - \cos \frac{\phi}{n}} e^{jk\rho \cos \phi} \\ \times \int_{\sqrt{k\rho a}}^{\infty} e^{-j\tau^2} d\tau + [\text{Higher Order Terms}]$$

where

$$a = 1 + \cos \phi$$

and  $n$  specifies the wedge angles  $(2-n)\pi$ .

For the half-plane, i. e.,  $n = 2$ , the higher order terms of Eq. (37) are identically zero.

The exact formulation based on an eigenfunction expansion may be used which converges rapidly for small values of  $\rho$

$$(38) \quad V_B(\rho, \phi, n) = \frac{1}{n} \sum_{m=0}^{\infty} \epsilon_m(j)^{\frac{m}{n}} J_{\frac{m}{n}}(k\rho) \cos \frac{m}{n} \phi \\ - \begin{cases} e^{jk\rho \cos \phi} & \phi < \pi \\ 0 & \phi > \pi \end{cases}$$

where  $J_{\frac{m}{n}}$  is the cylindrical Bessel function of order  $m/n$  and

$$\epsilon_m = \begin{cases} 1 & m = 0 \\ 2 & m \neq 0. \end{cases}$$

The solution to the plane wave diffraction, of a wedge with wedge angle  $(2-n)\pi$ , may be expressed in terms of a scalar function that represents the component of the electromagnetic field, normal to the plane of study in Fig. 12.

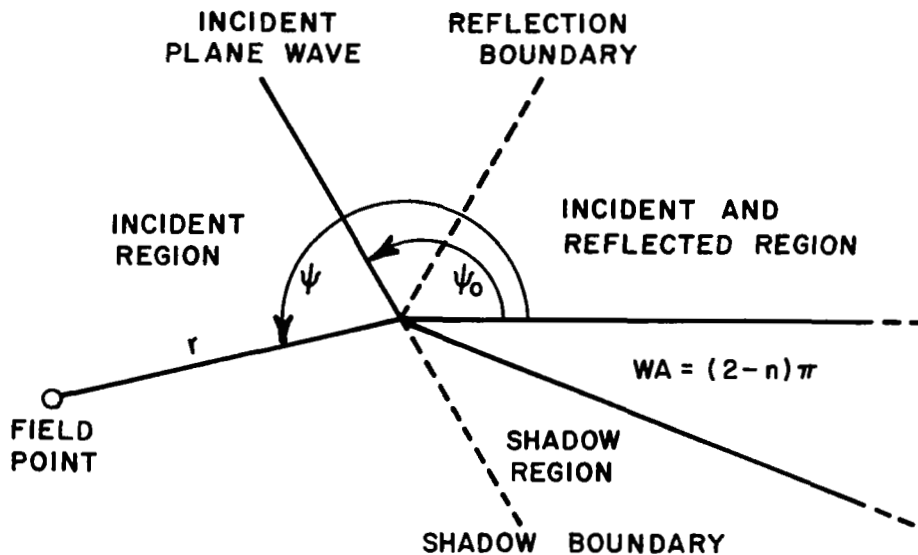


Fig. 12. Geometry of wedge diffraction.

The total field may be expressed as

$$(39) \quad U = U_o + U_d$$

For plane wave incidence the geometrical optics fields are

$$(40) \quad U_o = e^{jk\rho \cos(\psi - \psi_o)} \quad \text{incident region}$$

$$(41) \quad U_o = e^{jk\rho \cos(\psi - \psi_o)} + e^{jk\rho \cos(\psi + \psi_o)}$$

incident and  
reflected region

$$(42) \quad U_o = 0$$

shadow region

The diffracted field is given by

$$U_d = V_B(\rho, \psi - \psi_o, n) + V_B(\rho, \psi + \psi_o, n)$$

Since only the half-plane is employed in this publication, the following equations are restricted to  $n = 2$  for simplification.

For large values of  $k\rho(1 + \cos \phi)$

$$(43) \quad V_B(\rho, \phi, 2) \sim \frac{-e^{-j\left(k\rho + \frac{\pi}{4}\right)}}{2\sqrt{2\pi k\rho} \cos \frac{\phi}{2}}$$

In terms of this approximation, the radiation may be thought of as that from a line source at the edge radiating a cylindrical wave of the form  $K \frac{e^{-jk\rho}}{\sqrt{\rho}}$ . This line source concept is an extremely useful means of visualizing edge diffraction. The diffraction of a cylindrical wave by a wedge is illustrated in

Fig. 13.

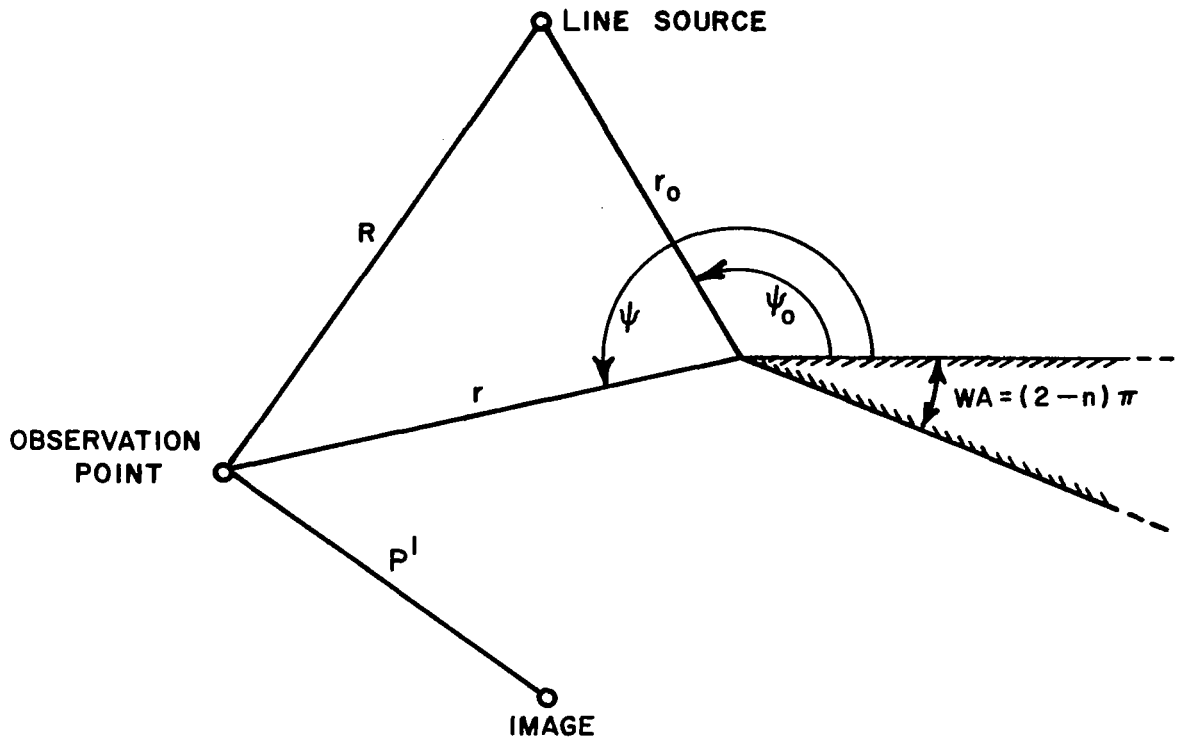


Fig. 13. Line source near field diffraction

The geometrical optics field in this case is given by

$$(44) \quad U_o = \frac{e^{-jkR}}{\sqrt{R}} = \frac{e^{-jk[r^2+r_o^2-2rr_o \cos(\psi-\psi_o)]^{\frac{1}{2}}}}{[r^2+r_o^2-2rr_o \cos(\psi-\psi_o)]^{\frac{1}{4}}}$$

incident region

$$(45) \quad U_o = \frac{e^{-jkR}}{\sqrt{R}} + \frac{e^{-jkR'}}{\sqrt{R'}} = \frac{e^{-jk[r^2+r_o^2-2rr_o \cos(\psi-\psi_o)]^{\frac{1}{2}}}}{[r^2+r_o^2-2rr_o \cos(\psi-\psi_o)]^{\frac{1}{4}}} + \frac{e^{-jk[r^2+r_o^2-2rr_o \cos(\psi+\psi_o)]^{\frac{1}{2}}}}{[r^2+r_o^2-2rr_o \cos(\psi+\psi_o)]^{\frac{1}{4}}}$$

incident and reflected

and

$$(46) \quad U_o = 0 \quad \text{shadow region}$$

The diffracted field is accurately given by<sup>8</sup>

$$(47) \quad U_d = \frac{e^{-jk(r+r_o)}}{\sqrt{r+r_o}} e^{jk \frac{rr_o}{r+r_o}} \left[ V_B \left( \frac{rr_o}{r+r_o}, \psi - \psi_o \right) + V_B \left( \frac{rr_o}{r+r_o}, \psi + \psi_o \right) \right] .$$

## APPENDIX B

The exact solution for the TEM mode radiation pattern of the parallel-plate waveguide, as shown in Fig. 1, is obtained by the Weiner-Hopf technique<sup>9</sup> and is given by

$$(48) \quad H_z(\rho, \theta) = \frac{e^{-j\left(k\rho - \frac{\pi}{4}\right)}_{kh} L_+(k) L_+(-k \cos \theta)}{\sqrt{2\pi k\rho}}$$

An expression for  $L_+(\alpha)$  which is valid for  $0 < \frac{kh}{2} < \pi$  is given by

$$(49) \quad L_+(\alpha) = \left\{ \left( \frac{\gamma h}{2} \right)^{-1} \sinh \left( \frac{\gamma h}{2} \right) \right\}^{\frac{1}{2}} \exp \left[ -\frac{1}{4} \alpha h - i \frac{\alpha h}{2\pi} \right. \\ \left. \left\{ 1 - 0.5772 + \ell n \left( \frac{4\pi}{kh} \right) \right\} - \frac{\gamma h}{2} \cos^{-1} \left( \frac{\alpha}{k} \right) \right. \\ \left. - i \sum_{n=1}^{\infty} \left\{ \frac{\alpha h}{2n\pi} - \psi_n \right\} \right]$$

where

$$\psi_n = \tan^{-1} \frac{\alpha}{\left\{ \left( \frac{2n\pi}{h} \right)^2 - k^2 \right\}^{\frac{1}{2}}}$$

For real values of  $\alpha$  and  $k$  and for  $-k < \alpha < k$  we have

$$(50) \quad \alpha = k \cos \lambda$$

$$(51) \quad \gamma = ik \sin \lambda$$

$$(52) \quad \cos^{-1}\left(\frac{\alpha}{k}\right) = \lambda$$

Therefore, the angular variation (with the factor  $\frac{e^{-j(k\rho + \frac{\pi}{4})}}{\sqrt{2\pi k\rho}}$  suppressed) is given by

$$(53) \quad R(\theta) = \left\{ \frac{\sin\left(\frac{1}{2} kh \sin \theta\right)}{\frac{1}{2} kh \sin \theta} \right\}^{\frac{1}{2}} kh e^{j\frac{\pi}{2}}$$

$$\exp\left[-\frac{1}{4} kh(1 - \cos \theta) - i \frac{kh(1 - \cos \theta)}{2\pi}\right]$$

$$\left\{ 1 - 0.5772 + \ln\left(\frac{4\pi}{kh}\right) - \frac{kh}{2} \theta \right.$$

$$- i \sum_{n=1}^{\infty} \left\{ \left( \frac{kh(1 - \cos \theta)}{2n\pi} \right) - \sin^{-1} \frac{kh}{2n\pi} \right.$$

$$\left. \left. + \tan^{-1} \frac{\cos \theta}{\sqrt{\left(\frac{2n\pi}{kh}\right)^2 - 1}} \right\} \right] .$$

## REFERENCES

1. Rudduck, R. C., "Application of Wedge Diffraction to Antenna Theory," Report 1691-13, 30 June 1965, ElectroScience Laboratory (formerly Antenna Laboratory), The Ohio State University Research Foundation; prepared under Grant Number NsG-448, National Aeronautics and Space Administration, Office of Grants and Research Contracts, Washington, D. C.
2. Ryan, C. E., Jr., Rudduck, R. C., "Calculation of the Radiation Pattern of a General Parallel-Plate Waveguide Aperture for the TEM and TE<sub>01</sub> Waveguide Modes," Report 1693-4, 10 September 1964, ElectroScience Laboratory (formerly Antenna Laboratory), The Ohio State University Research Foundation; prepared under Contract N62269-2184, U. S. Naval Air Development Center, Johnsville, Pennsylvania.
3. Yu, J. S., Rudduck, R. C., "Higher-Order Diffraction Concept Applied to Parallel-Plate Waveguide Patterns," Report 1691-16, 15 October 1965, ElectroScience Laboratory (formerly Antenna Laboratory), The Ohio State University Research Foundation; prepared under

Grant Number NsG-448, National Aeronautics and Space Administration, Office of Grants and Research Contracts, Washington, D. C.

4. Mikuteit, S., "Mutual Coupling in a Three-Element, Parallel-Plate Waveguide Array by Wedge Diffraction and Surface Integration Techniques," Report 2485-1, (in preparation), ElectroScience Laboratory (formerly Antenna Laboratory), The Ohio State University Research Foundation; prepared under Contract N62269-67-C-0582, Department of the Navy, U. S. Naval Air Development Center, Johnsville, Warminster, Pa.
5. Harrington, R. F., Time-Harmonic Electromagnetic Fields, McGraw-Hill Book Co., Inc., New York, 1961 pp. 103-116.
6. Sommerfeld, A., Optics, Academic Press, Inc., New York, 1954, pp. 245-265.
7. Papoulis, A., The Fourier Integral and its Applications, Electronic Science Series, McGraw-Hill Book Co., Inc., 1962.
8. Tsai, L. L., Rudduck, R. C., "Accuracy of Approximate Formulations for Near Field Wedge Diffraction of a Line Source," Report 1691-18, 15 March 1966, ElectroScience Laboratory (formerly Antenna Laboratory), The Ohio State

University Research Foundation; prepared under Grant  
Number NsG-448, National Aeronautics and Space  
Administration, Office of Grants and Research Contracts,  
Washington, D. C.

9. Noble, B. , Method Based on the Weiner-Hopf Technique  
for the Solution of Partial Differential Equations,  
Pergamon Press, New York, 1958, pp. 105-110 and p. 127.